Available online at www.sciencedirect.com
ScienceDirect
Journal of Sound and Vibration 325 (2009) 145–160
JOURNAL OF SOUND AND VIBRATION
www.elsevier.com/locate/jsvi

Nonlinear dynamic analysis of cylindrical roller bearing with flexible rings

Alexandre Leblanc*, Daniel Nelias, Cyril Defaye

LaMCos, UMR CNRS 5259, INSA Lyon, 69621 Villeurbanne, France

Received 13 November 2008; received in revised form 11 March 2009; accepted 11 March 2009
Handling Editor: C.L. Morfey
Available online 16 April 2009

Abstract

A nonlinear plan dynamic model for cylindrical bearings has been developed, predicting the interaction forces between the retainers and the rolling elements. Roller–race contacts are analyzed in detail and resulting forces and moments are determined. An elastohydrodynamic lubrication (EHL) model provides the traction components while a hydrodynamic formulation is used for the roller–cage interactions. Structural deformations of the rings are included in the geometrical equations linking the relative displacements between rings. The Newmark type implicit integration technique coupled with the Newton–Raphson method is used to solve the differential equation system iteratively. Time displacements and theirs FFT are used to illustrate and elucidate the diversity of the system response.

Computations performed when considering the structural deformations of the rings show a low frequency shift, as higher harmonics are attenuated while the first are more pronounced. With an unbalanced rotor, the ball pass frequency (BPF) is modulated with this perturbation leading to an aperiodic response. This is particularly true for the counter-rotating bearing investigated. Finally, results for different cage materials show a significant influence only on the cage center location, whereas the inertia moment of the cage is of little impact on the global dynamics behavior.

1. Introduction

The dynamical analysis of a rotor system supported by rolling bearings is of prime importance in many engineering applications. Rotors are often subjected to either stationary radial load or periodic forces due to unbalanced mass. The nonlinear behavior of rolling bearings should be considered carefully when looking at the shaft trajectory or the dynamic response of the rotor-bearing system. The numerical simulation of a rolling bearing submitted to transient loading will improve our understanding of the dynamic response of the whole system. It is now clear that, when a roller bearing is radially loaded, part of the rollers are unloaded as they whirl in orbit. It is then interesting to look at the behavior of each roller when it enters and exits the loading zone. Factors such as the interactions between the cage and the rollers or the irregular traction characteristics further act on the motion of the bearing elements, leading sometimes to instabilities. Beyond these

*Corresponding author.
E-mail addresses: ale.leblanc@gmail.com (A. Leblanc), daniel.nelias@insa-lyon.fr (D. Nelias).

0022-460X/$ - see front matter © 2009 Elsevier Ltd. All rights reserved.
doi:10.1016/j.jsv.2009.03.013

Nomenclature

A	cross-sectional area
CC	cage/ring friction torque
CC_j	roller end/cage pocket flange friction torque
CE	roller end/guiding flange friction torque
CP	rolling resisting moment at the roller/ring contact
d	diameter
d_m	bearing pitch diameter
E	moduli of elasticity
EX	cage eccentricity
F	friction force at the roller/ring contact
F_c	roller centrifugal force
F_R	radial load
FC_1	traction force at front roller/pocket
FC_2	traction force at rear roller/pocket
FE	friction force at the roller end/ring guiding flange
FOL	oleodynamic drag force acting on the roller
h_i	EHL lubricant film thickness at roller/inner ring contact
h_o	EHL lubricant film thickness at roller/outer ring contact
H_1	lubricant film thickness between the roller and the cage
I	area moment of inertia of the cross-sectional area
J_d	bearing diametrical clearance
K	stiffness coefficients
L	load
m	mass
N	number of roller
Q	normal load at the roller/ring contact
QC	normal load at the cage/ring contact (short journal bearing effect)
QC_1	front roller/cage pocket contact
QC_2	rear roller/cage pocket contact
r	radius
R_r	roller radius
VX	horizontal linear velocity
VY	vertical linear velocity
X	horizontal position
Y	vertical position
δ	contact deformation
v	Poisson's ratio
ρ	density
υ	structural deformation
υ_c	diametral growth
ϕ	cage attitude angle
Ψ	angular position
ω	angular speed

Subscripts

i	inner ring
o	outer ring
c	cage
j	roller number
R	roller

phenomena, responses of nonlinear systems often show unexpected behavior and are extremely sensitive to initial conditions, like clearance or excitation by unbalanced rotors.

Until the late 1970s, most of the analytical simulations of rolling-element bearings were restricted to quasi-static models which consist of a set of nonlinear algebraic equations solved by standard iteration methods. Walter [1] was the first to develop an analytical model for ball bearing and cage dynamics. Later, Gupta [2,3] modified and extended this analysis to other types of rolling element bearings, setting the basis of the well-known computer code ADORE©, which has been used to validate the model presented in this paper. As a result of the increase in capacities, the number of publications in the field has grown significantly over the years.

A lot of research has been conducted on three-dimensional modeling [2,4–7], the effects of geometrical imperfections [8,9] and experimental results [10,11]. More recently, Lee et al. [12] derived a theoretical model for the coupling-rotor–ball bearing systems with misalignment and showed the whirling orbits' tendency to collapse with increasing angular misalignment. Tiwari et al. studied the nonlinear behaviors of a balanced [13] or unbalanced [14] rotor due to the effect of internal clearance of the ball bearing. Harsha et al. [15] simulated some dynamic responses for rotors supported by ball bearings, using a 2 dof model with clearance and waviness. Similar investigations have been conducted with a 5 dof transient dynamic model considering the centrifugal force and gyroscopic moment of the ball by Changqing et al. [16]. For a rotating system supported

by bearings, the impact of ball waviness on the resulting sideband frequencies has been investigated by Jang et al. [17].

This non-exhaustive list of dynamic analysis for rolling-element demonstrates the variety of phenomena that may affect the vibration behavior of such systems. The present paper contains a two-dimensional roller bearing dynamic analysis which takes into account some of the forsaken parameters: the effects of unbalanced rotor forces, cage materials and counter-rotating motions are investigated while also considering the structural deformations of the inner- and outer-rings.

2. The problem formulation

A schematic diagram of roller bearing is shown in Fig. 1. The elastic deflection at the contact between a crowned roller and a ring was determined by Palmgren [18]. This local or contact deformation is independent of the structure deformation.

2.1. Structural deformations

The proposed solution is an extension of the model proposed by Cavallaro et al. model [19]. The global or structural deformation has two contributions: a uniform centrifugal expansion and the load distribution among rollers. Both are used to obtain the operating radial clearance, i.e. the difference between the outer and inner ring radii minus the roller diameter.

The centrifugal expansion affecting both the cage and the rotating ring is given by Hirotoshi et al. [20]:

$$\upsilon_{ci} = \frac{\rho\Omega^2}{4E}((1-\nu)(3+\nu)(r_i^2 - r_o^2) + (1+\nu)(3+\nu)r_o^2 - (1-\nu^2)r_i^2)r_i \tag{1}$$

$$\upsilon_{co} = \frac{\rho\Omega^2}{4E}((1-\nu)(3+\nu)(r_i^2 - r_o^2) + (1+\nu)(3+\nu)r_i^2 - (1-\nu^2)r_o^2)r_o \tag{2}$$

where υ_{ci} and υ_{co} are the diametral growths at the inner and outer radii, r_i and r_o, respectively. In the present model, the centrifugal expansion is included in the diametral clearance J_d.

The ring out-of-roundness $\upsilon(\theta)$ produced by a single line contact can be expressed through a Fourier series as follows:

$$\upsilon(\theta) = L\sum_{k=0}^{\infty} K_k \cos(k\theta) \tag{3}$$

Superposing the effect of N equidistant loads (L_j) yields

$$\upsilon(\theta) = \sum_{j=1}^{N} L_j \sum_{k=0}^{\infty} K_k \cos(k(\Psi_j - \theta)) \tag{4}$$

where each contact load coincides with the roller angular position Ψ_j (cf. Fig. 2).

The stiffness coefficients K_k can be obtained from an analytical solution as the one given by Young [21]: assuming a single load is applied, the thin ring is balanced by a symmetric tangential shear stress distribution.

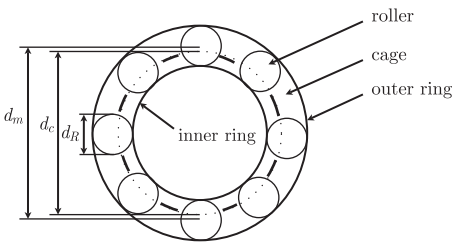

Fig. 1. Schematic diagram of a roller bearing.

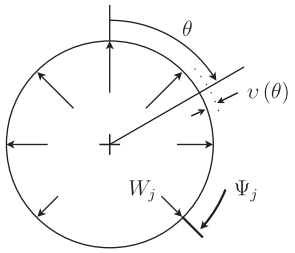

Fig. 2. Roller/ring load distribution for a radially loaded bearing.

Only three stiffness coefficients are then required to obtain the ring deformations:

$$\upsilon(\theta) = L(K_0 + K_1 \cos\theta + K_2 \cos 2\theta) \tag{5}$$

Although this formula leads to a good approximation of the shape of the inner ring when subjected to a static load, it fails completely for a set of equally, or almost identically loaded rollers. This is the case for the outer ring, for high-speed application, since the rollers are all loaded at least by the centrifugal force.

For a thin ring submitted to N equivalent (F_c) loads, several analytical solutions are available. Yhland's formulation is used here (as reported by Wensing [22]). This solution, valid at any point of the ring, takes into account the flexural and the extensional deformations:

$$\upsilon_Y(\theta) = \frac{F_c \times N \times r_o}{2\pi E \times A_o} + \frac{F_c \times N \times r_o^3}{\pi E \times I_o} \sum_{q=1}^{\infty} \frac{1}{((qN)^2 - 1)^2} \cos(qN\theta) \tag{6}$$

For the complete loading of the outer ring, this yields

$$\upsilon(\theta) = \sum_{j=1}^{N} (Q_{oj} - F_c) \sum_{n=0}^{2} K_n \cos(n(\phi_j - \theta)) + \upsilon_Y(\theta) \tag{7}$$

2.2. Equations of motion

The roller bearing behavior is described by solving a set of dynamic, equilibrium and geometric nonlinear equations, including both cage and lubricant effects. The problem is planar, so only pure radial loading is considered, assuming perfect geometry for the rolling elements and no ring misalignment.

Fig. 3 shows a roller loaded at the roller/race contact (Q), at the front or rear roller/cage pocket contact (QC_1 and QC_2, respectively), and submitted to a centrifugal force (F_c). Dry or lubricated traction forces at the roller/race and roller/pocket (F, FC_1 and FC_2, respectively) are of primary importance in roller equilibrium. A resisting torque (CP) due to an asymmetric hydrodynamic pressure field and the oleodynamic drag force (FOL) are considered. Due to small internal clearances needed for high-speed operation, friction effects at the roller end/cage pocket (friction torque CC) and roller end/guiding flange (traction force FE and friction torque CE) are also considered.

In addition to the roller/cage interactions, the contact between the cage and the guiding ring surfaces introduces a normal load (QC) and a friction torque (CC) linked to the cage attitude angle (ϕ) and eccentricity (EX), through a short journal bearing model (see Fig. 4).

Finally, the roller/ring reaction forces balance the inner ring. See Cavallaro paper [19] for details on force models used.

For the roller j, the application of the Newton's second law yields

$$m_r \frac{d_m}{2} \frac{\mathrm{d}\omega_j}{\mathrm{d}t} = QC_{2j} - QC_{1j} - FOL + F_{ij} - F_{oj} + FE_j \tag{8}$$

$$J_r \left(\frac{\mathrm{d}\omega_j}{\mathrm{d}t} + \frac{\mathrm{d}\omega_{R_j}}{\mathrm{d}t} \right) = RR(FC_{1j} + FC_{2j} - F_{ij} - F_{oj}) + CE_j + CC_j + CP_{ij} + CP_{oj} \tag{9}$$

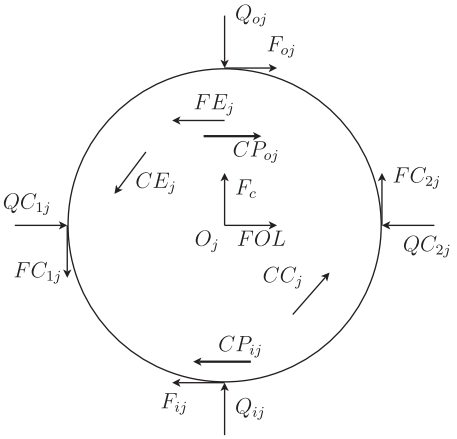

Fig. 3. Loads acting on a roller.

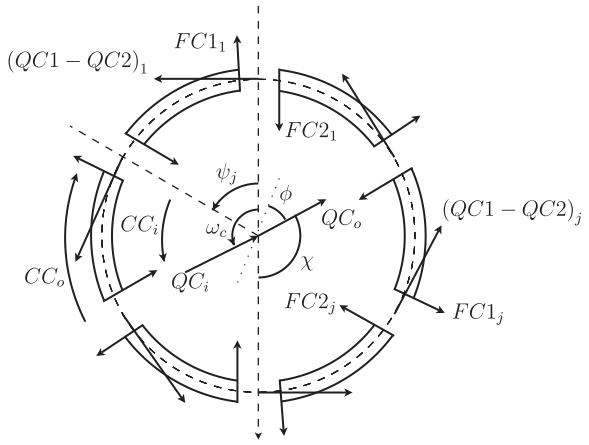

Fig. 4. Loads acting on the cage.

with

$$\frac{\mathrm{d}\Psi_j}{\mathrm{d}t} = \omega_j \tag{10}$$

Similarly, for the cage:

$$m_c \frac{\mathrm{d}VX_c}{\mathrm{d}t} = \sum_{j=1}^{N}((QC_{2j} - QC_{1j})\cos\Psi_j + (FC_{2j} + FC_{1j})\sin\Psi_j) + (QC_i + QC_o)\sin\chi \tag{11}$$

$$m_c \frac{\mathrm{d}VY_c}{\mathrm{d}t} = \sum_{j=1}^{N}((QC_{2j} - QC_{1j})\sin\Psi_j + (FC_{2j} - FC_{1j})\cos\Psi_j) - (QC_i + QC_o)\cos\chi \tag{12}$$

$$J_c \frac{\mathrm{d}\omega_c}{\mathrm{d}t} = \sum_{j=1}^{N}\left((QC_{2j} - QC_{1j})\frac{d_m}{2} - (FC_{2j} + FC_{1j})RR - CC_j\right) + CC_i - CC_o - EX \cdot QC_i \sin\chi \tag{13}$$

with

$$\frac{d\Psi_c}{dt} = \omega_c; \quad \frac{dX_c}{dt} = VX_c; \quad \frac{dY_c}{dt} = VY_c \tag{14}$$

For the inner ring:

$$m_i \frac{dVX_i}{dt} = \sum_{j=1}^{N} (Q_{ij} \sin \Psi_j) - F_{ur} \sin(\omega_i t) \tag{15}$$

$$m_i \frac{dVY_i}{dt} = -\sum_{j=1}^{N} (Q_{ij} \cos \Psi_j) + F_R + F_{ur} \cos(\omega_i t) \tag{16}$$

where $F_{ur} = m_{ur} E X_{ur} \omega_i^2$ and with

$$\frac{dX_i}{dt} = VX_i; \quad \frac{dY_i}{dt} = VY_i \tag{17}$$

One equation is added for each roller:

$$0 = FC_{2j} - FC_{1j} + Q_{ij} - Q_{oj} + F_c \tag{18}$$

where $F_c = m_R d_m \omega_j^2 / 2$.

2.3. Geometry considerations

Two geometric relations must be added to describe the relative displacement between the inner and the outer ring centers (Fig. 5) and the lubricant film thickness between the roller and the cage pocket. The first relation includes the elastohydrodynamic lubrication (EHL) film thickness at the roller/race contacts h, the

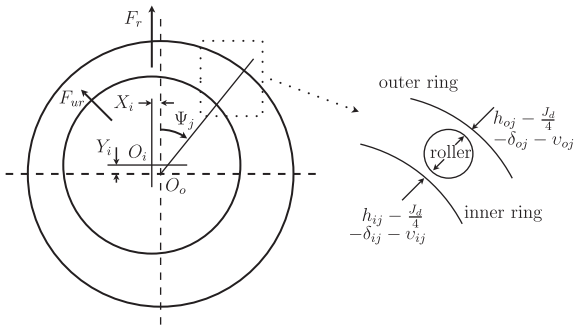

Fig. 5. Relative displacement between the inner and the outer ring centers.

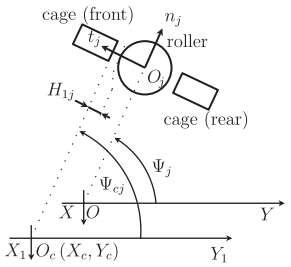

Fig. 6. Lubricant thickness between the roller and the cage.

contact deformations δ, the radial clearance J_d and the structural deformations υ:

$$\frac{J_d}{2}+\delta_{ij}+\delta_{oj}-h_{ij}-h_{oj}+\upsilon_{ij}+\upsilon_{oj}=Y_i\cos\Psi_j-X_i\sin\Psi_j \tag{19}$$

The lubricant film between the roller and the cage (Fig. 6) is given by

$$H_{1j}=\frac{d_m}{2}\left(\Psi_{cj}-\arctan\left(\frac{2R_r}{d_m}\right)-\arctan\left(\frac{\frac{X_c}{EX}\cos\Psi_{cj}+\frac{Y_c}{EX}\sin\Psi_{cj}}{\frac{R_c}{EX}-\left(\frac{X_c}{EX}\sin\Psi_{cj}-\frac{Y_c}{EX}\cos\Psi_{cj}\right)}-\Psi_j\right)\right) \tag{20}$$

where $\Psi_{cj}=\Psi_c+2\pi(j-1)/N$.

2.4. Validations

The basic testing of the present code has been performed with ADORE© [3] and with the research model used by Ghaisas et al. [23]. Fig. 7 shows the correlation coefficients for the radial displacements predicted by Gupta's software and our model applied on a perfect roller bearing with radial loading [3, Table 8-3]. High rate of agreement is achieved for the inner ring trajectories and for the speed range investigated. The cage behavior still correctly predicted although cage interactions differ somewhat for the two models.

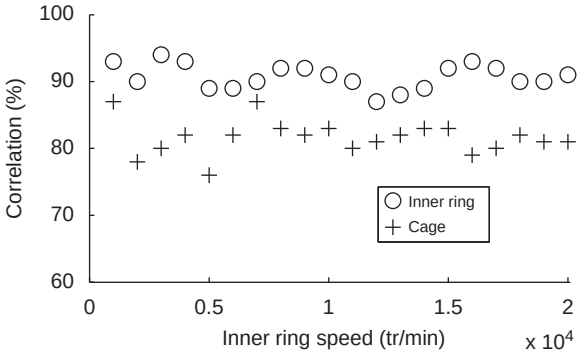

Fig. 7. Correlation of the radial displacements predicted by the present model and ADORE©.

Table 1
Bearing parameters.

Number of rollers $N=28$
Pitch diameter d_m (mm) = 144.5
Cage diameter d_c (mm = 140.7
Roller diameter d_R (mm) = 12
Inner shaft + ring thickness (mm) 41
Outer shaft + ring thickness (mm) 30
Free diameter clearance J_d (mm) = 6E−2
Race and roller material = M50
Cage material: M50 or Peek
Cage centering: inner ring
Oil: mobil oil jet II (MIL-L-23699)

3. Results

The equations of motion are solved using a modified Newmark-β method to investigate the effects of internal clearance, ring asymmetry and cage material. A large number of revolutions is

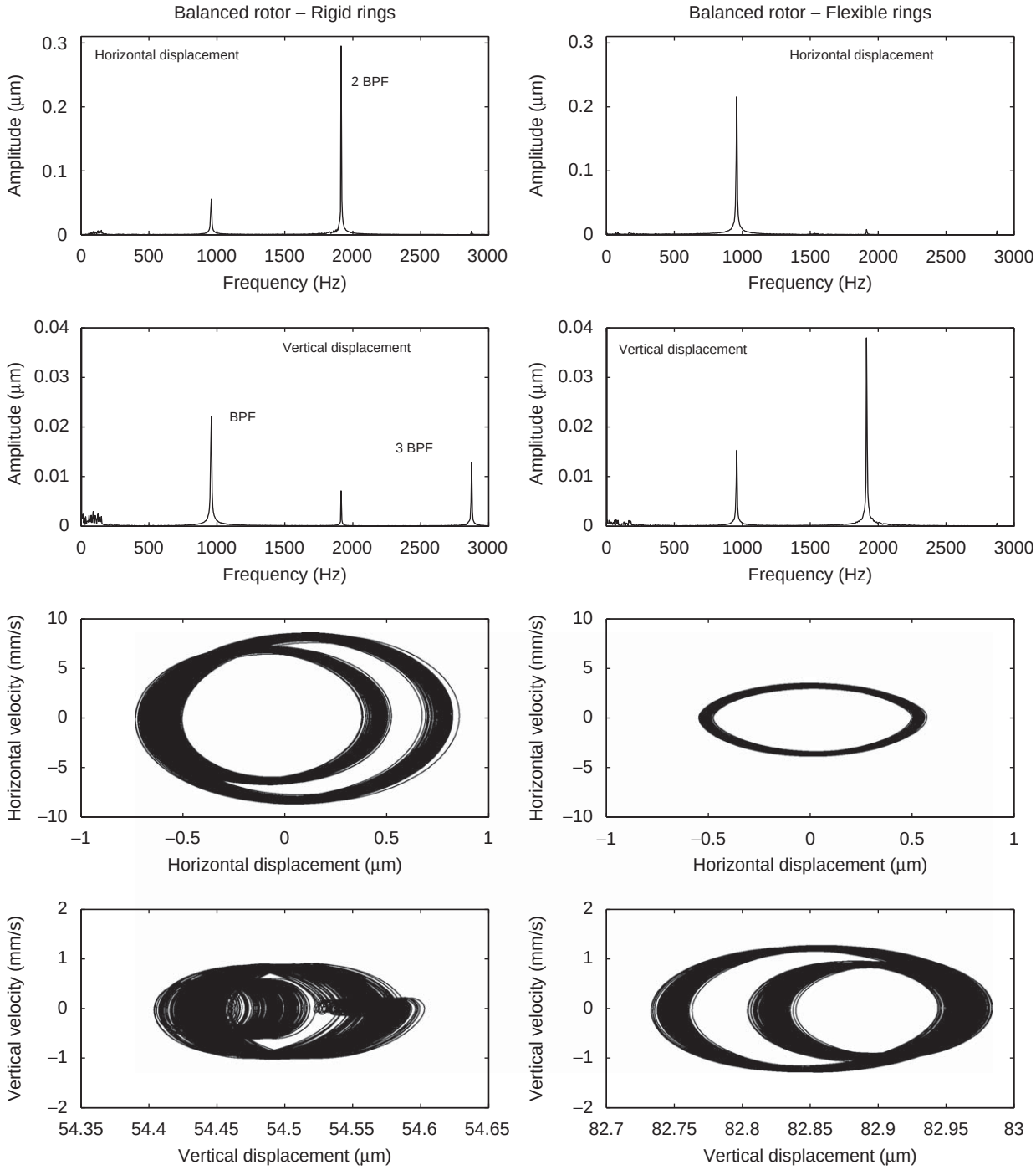

Fig. 8. Inner ring displacements at 4500 rev/min for $F_r = 3000$ daN with rigid and flexible rings—balanced rotor.

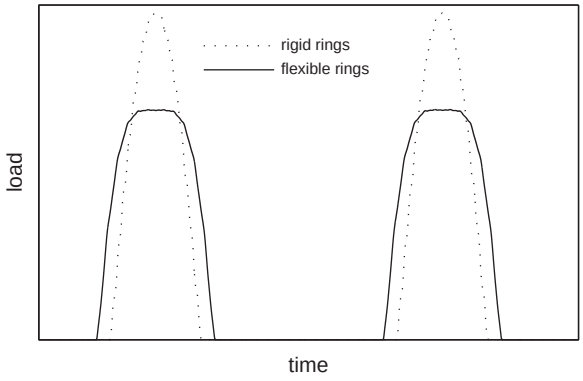

Fig. 9. Roller load shape.

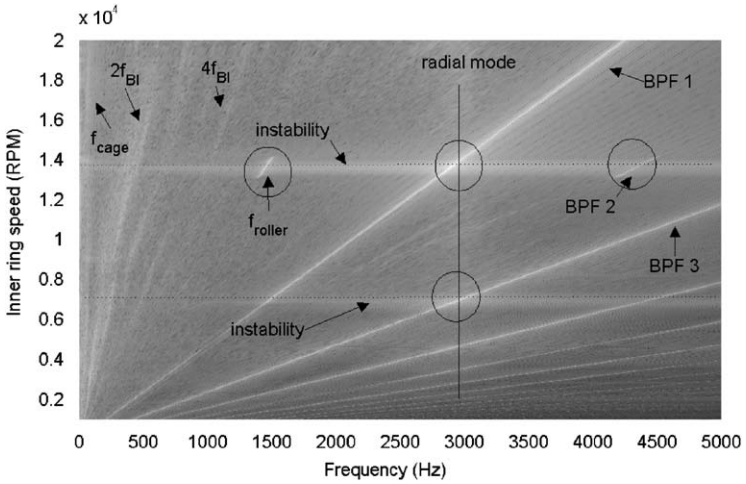

Fig. 10. Campbell diagram for the radial displacement of the inner ring—rigid rings.

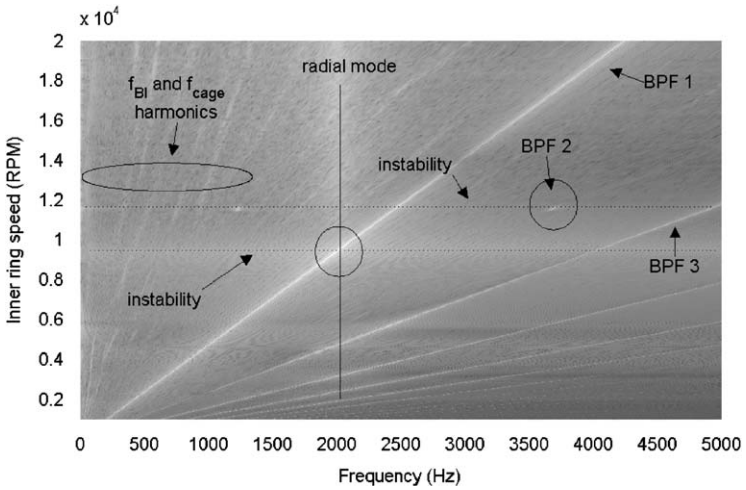

Fig. 11. Campbell diagram for the radial displacement of the inner ring—flexible rings.

computed to ensure a steady-state response. The displacement and velocity of the bearing elements are recorded at each time step. The characteristics of the roller bearing investigated are given in Table 1.

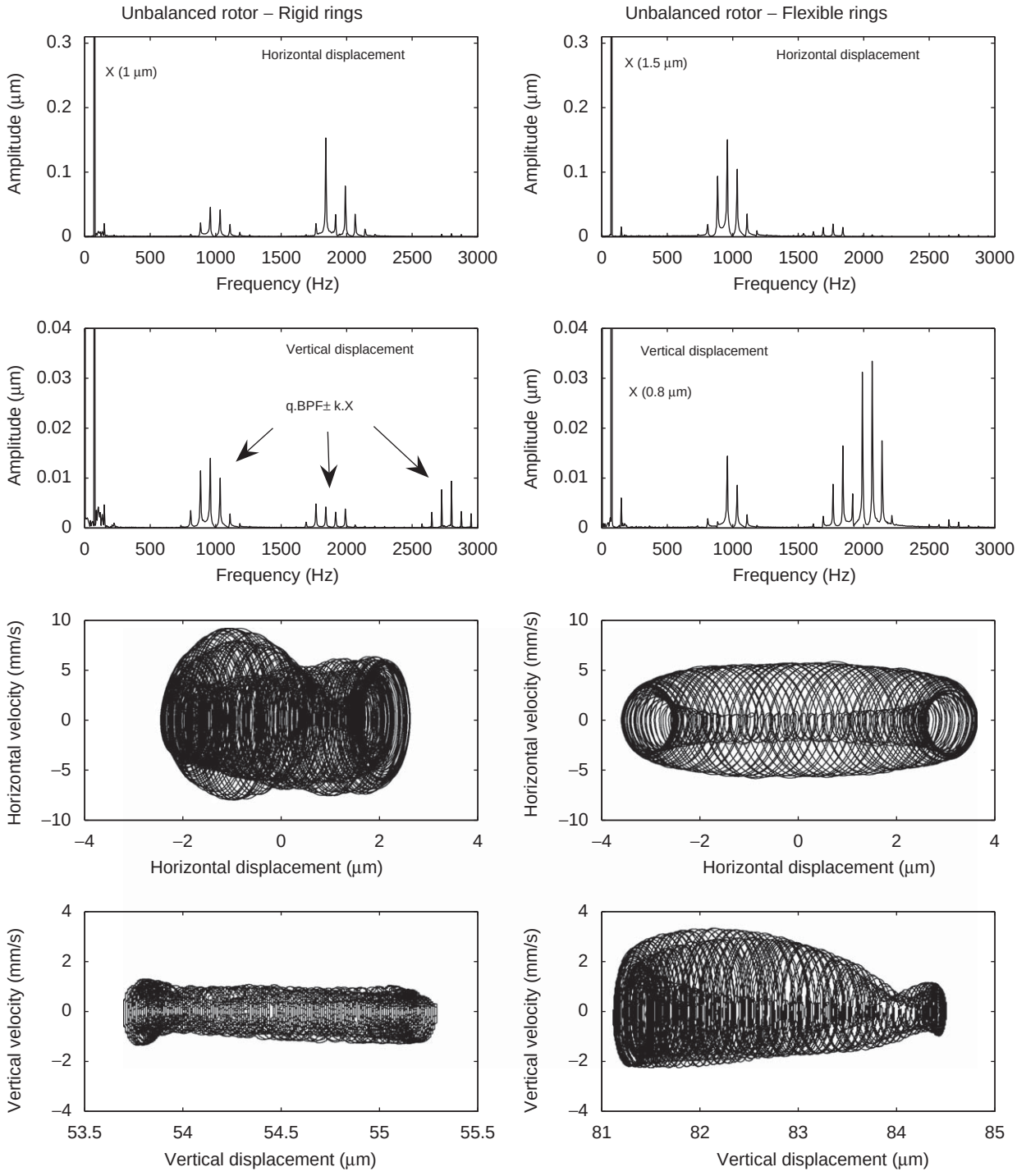

Fig. 12. Inner ring displacements at 4500 rev/min for $F_r = 3000$ daN with rigid and flexible rings—unbalanced rotor.

3.1. Initial conditions

For nonlinear systems, different initial conditions lead to different behaviors and solutions. The choice of time step δt is a key point: it should be small enough to get an accurate numerical solution

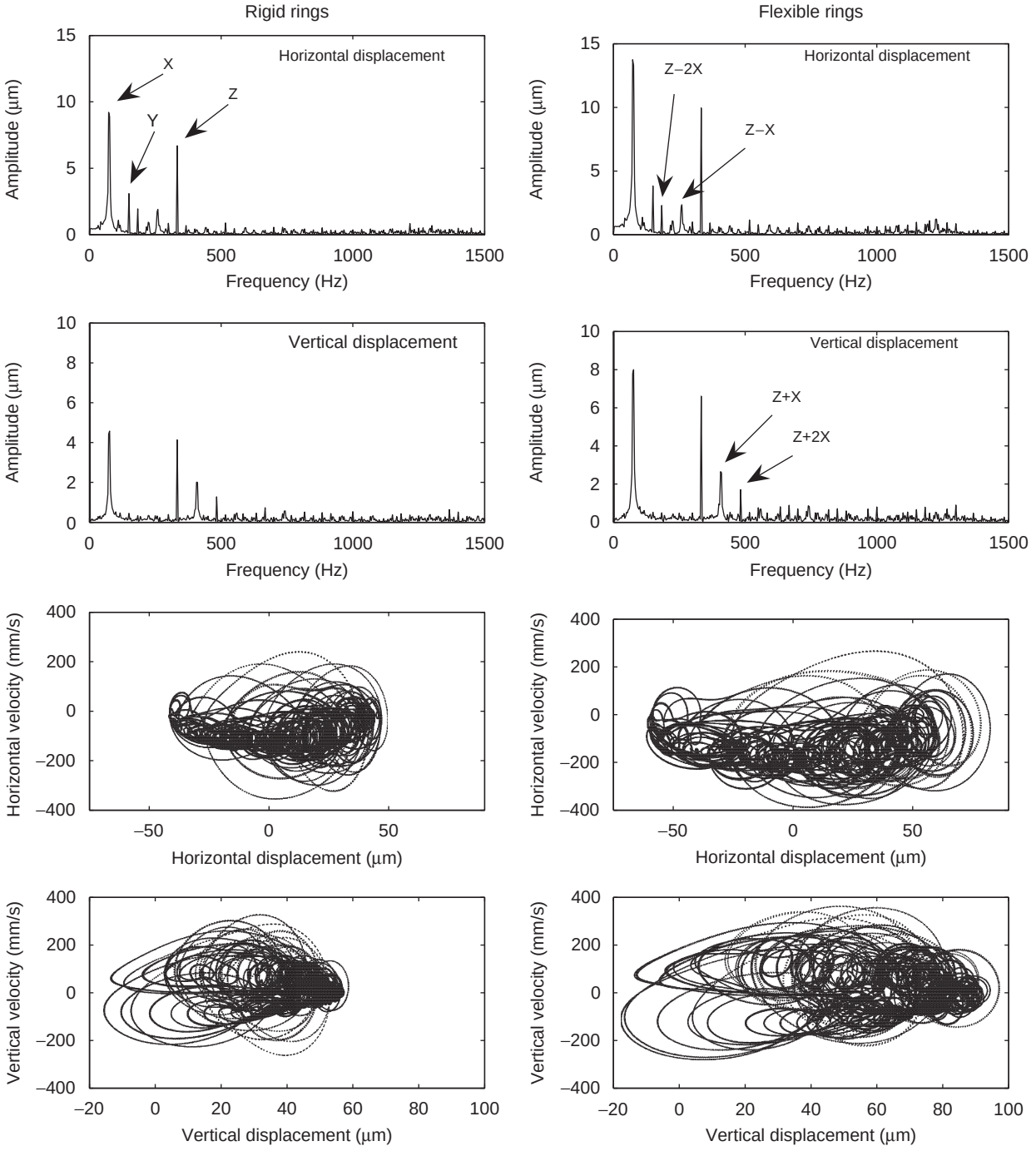

Fig. 13. Inner ring displacements at $\omega_i = 4500\,\text{rev/min}$ and $\omega_0 = 20,000\,\text{rev/min}$ for $F_r = 1500\,\text{daN}$ with rigid and flexible rings—unbalanced counter-rotating bearing.

but large enough to avoid significant truncation errors and keep the computational solution reasonable. Here, δt is set to 5–10 μs and at time $t = 0$, the initial bearing parameters are those given by the quasi-static equilibrium.

3.2. Flexible rings

Fig. 8 shows the rotor mass center for rigid (left) or flexible (right) rings. As the average speed of a roller around the outer race is equal to cage speed ω_c, the rotor is excited at the frequency of $N\omega_c$, known as "ball" pass frequency (BPF). Here the BPF is equal to 960 Hz. For the rigid ring case, the applied radial load is supported by a few rollers located in a narrow angular region, depending only on the elastic deflection at the roller/raceway contact. These peak-shaped load profiles induce the strong second harmonic of BPF for the horizontal displacement. For the vertical displacement, a third harmonic contributes to the response. This frequency is directly linked to the short loading period of the rollers. With the flexible rings, higher harmonics disappear as the load period increases while the contact pressure distribution is flattened (cf. Fig. 9).

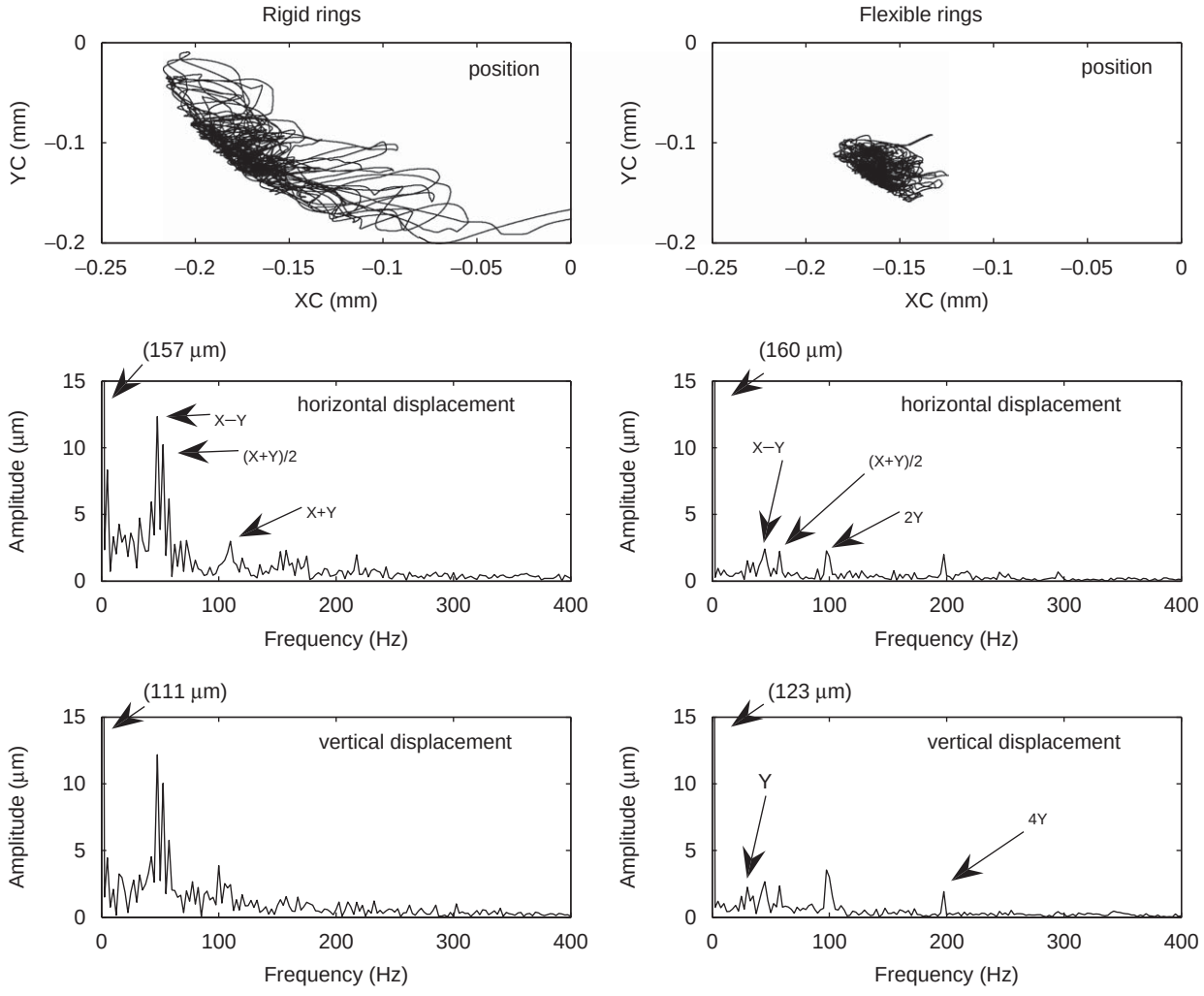

Fig. 14. Steel cage position at 4500 rev/min for $F_r = 15,000$ N—balanced rotor.

3.3. Stability analysis

In Fig. 8, a band of low frequency is visible in each of the displacement responses. It can be suspected at first to be the result of numerical errors. To dispel these errors and to find any critical values leading to dramatic bearing behavior, a stability analysis is performed. In Figs. 10 and 11 the Campbell diagrams are shown for the radial displacements of the inner ring of Fig. 8 for rotating speed from 1000 to 20,000 rev/min with 100 rev/min step.

Aside the BPF harmonics found previously, two instability rotating speeds areas are found in the investigated range. For the rigid case shows in the Fig. 10, the first instability area is around 7 krev/min and the second around 14 krev/min. A radial mode is also slightly apparent at 3 kHz while the lower band of frequencies contains several harmonics linked to the cage (f_{cage}), roller (f_{roller}) and inner ring (f_{IR}) frequencies. The flexibility of the rings (Fig. 11) shifts the radial mode near 2 kHz due to this severe damping. Instability areas are also altered and the rolling element harmonics appear more clearly on the lower frequency band.

3.4. Unbalanced rotor

The level of the unbalanced force has been taken as 5% of F_r. Response plots have been generated for the rigid and flexible ring cases as shown in Fig. 12. Aside from the new fundamental at $X = 75$ Hz ensuing from

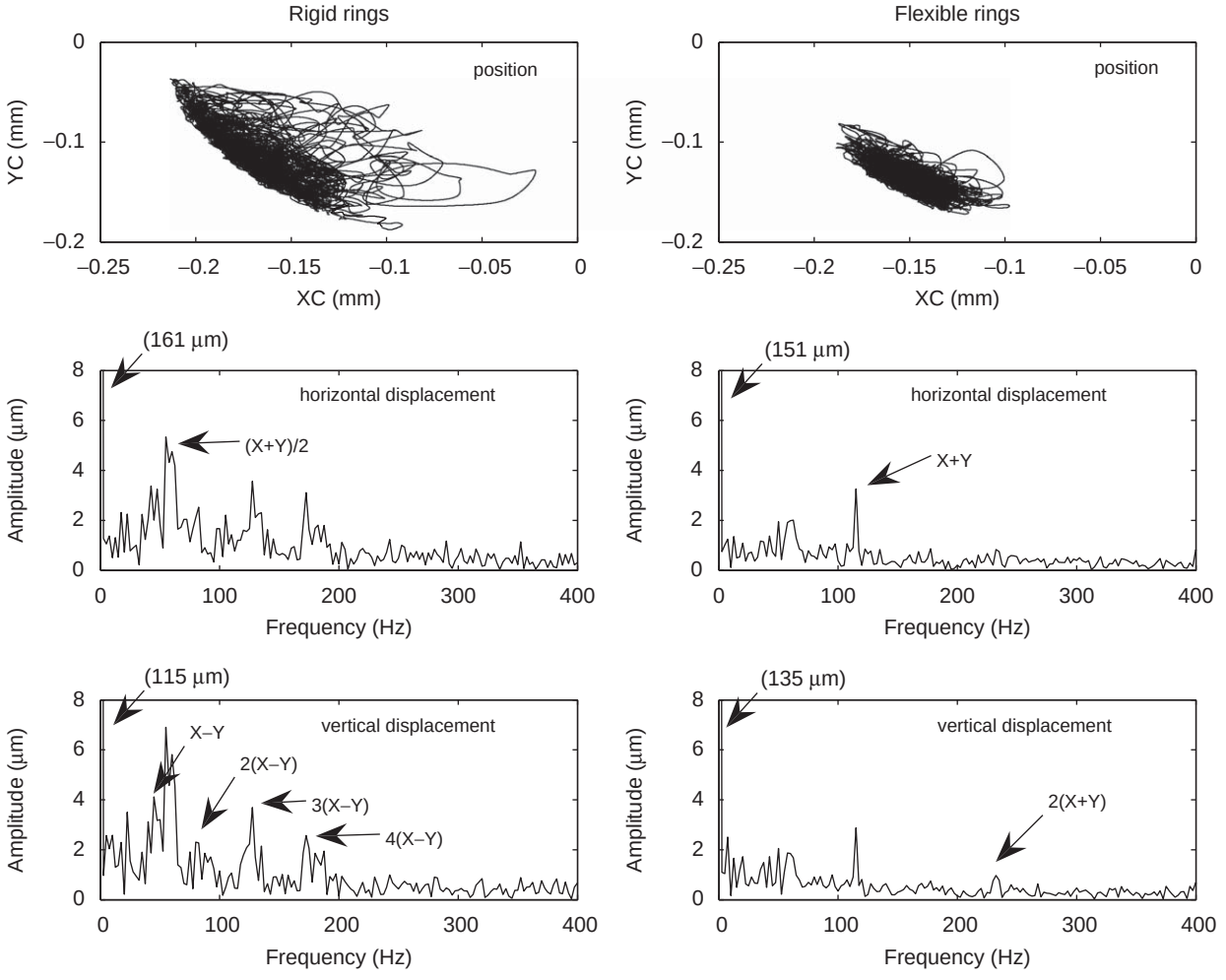

Fig. 15. Peek cage position at 4500 rev/min for $F_r = 15,000$ N—balanced rotor.

the unbalanced rotor, the BPF peak frequencies and harmonics are found to be similar to those previously obtained, although they are modulated by the rotor speed.

In turbomachinery, the inter-shaft bearings can operate with a counter-rotating motion with important unbalanced forces on each of the rings. Fig. 13 shows the studied roller bearing with an outer ring rotating at 20,000 rev/min ($Z = 233$ Hz). Here the radial static force F_r is set to 1500 daN, the inner unbalanced force to $\frac{2}{3}$ of F_r and the outer unbalanced force to $\frac{1}{3}$ of F_r. These unbalanced forces become predominant for the response of the inner ring, since the principal harmonics are function of the rings' speeds. The BPF is no longer visible and a strong harmonic at cage speed ($Y = 150$ Hz) appears to underline the influence of the static load.

3.5. Cage material

Two cage materials are investigated: steel and carbon fiber reinforced Peek (polyetheretherketones). Peek is a thermoplastic which offers a significant gain on cage weight (almost 20% for this bearing) with excellent mechanical properties. The small inertia of Peek cages is useful to reduce the impact loads between the roller and the retainer. However it may lead to some cage instabilities. Figs. 14–17 highlight the effects of the retainer material on cage position, for rigid (left) or flexible (right) rings, with balanced and severely unbalanced rotors (80% of F_r).

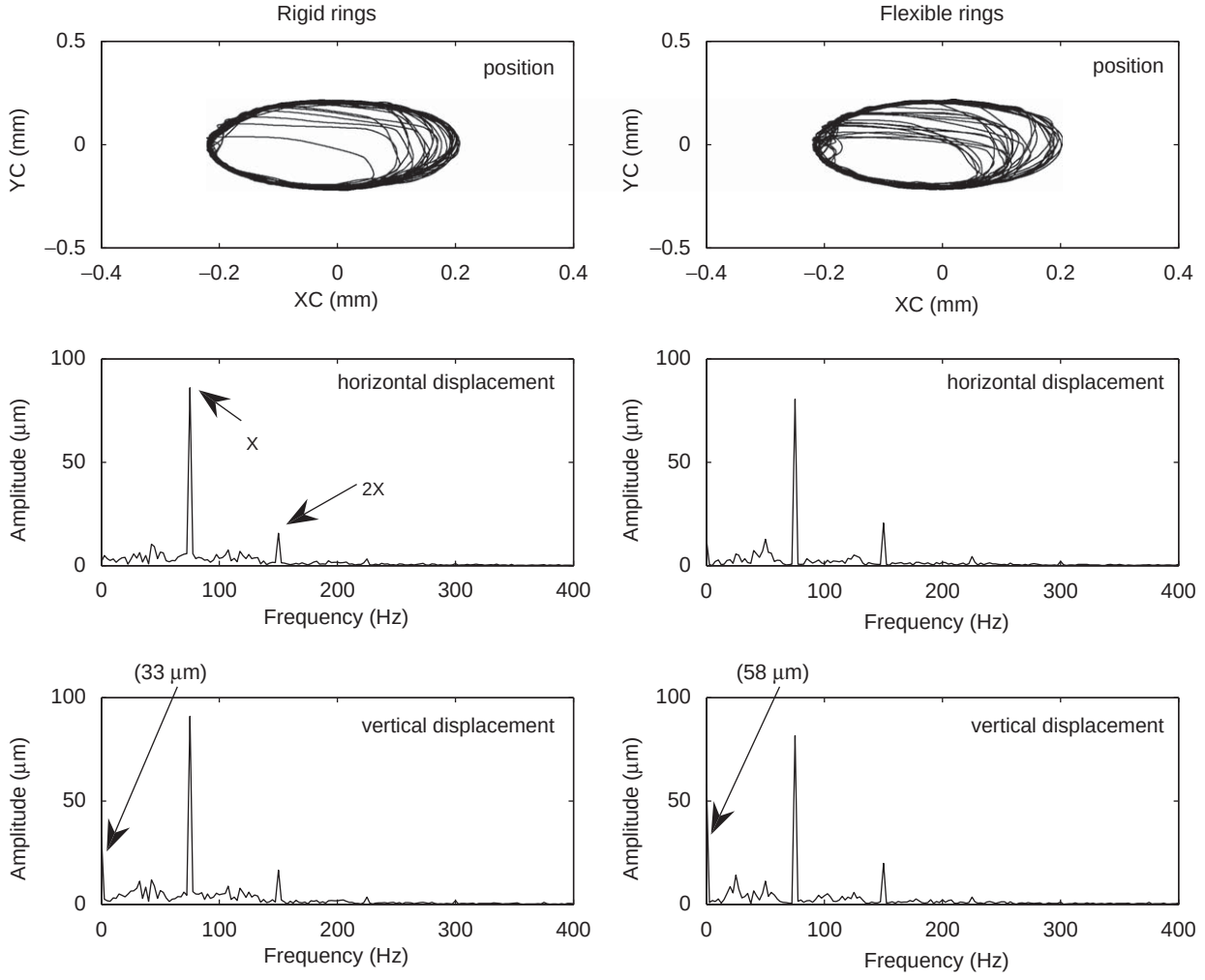

Fig. 16. Steel cage position at 4500 rev/min for $F_r = 15,000$ N—unbalanced rotor.

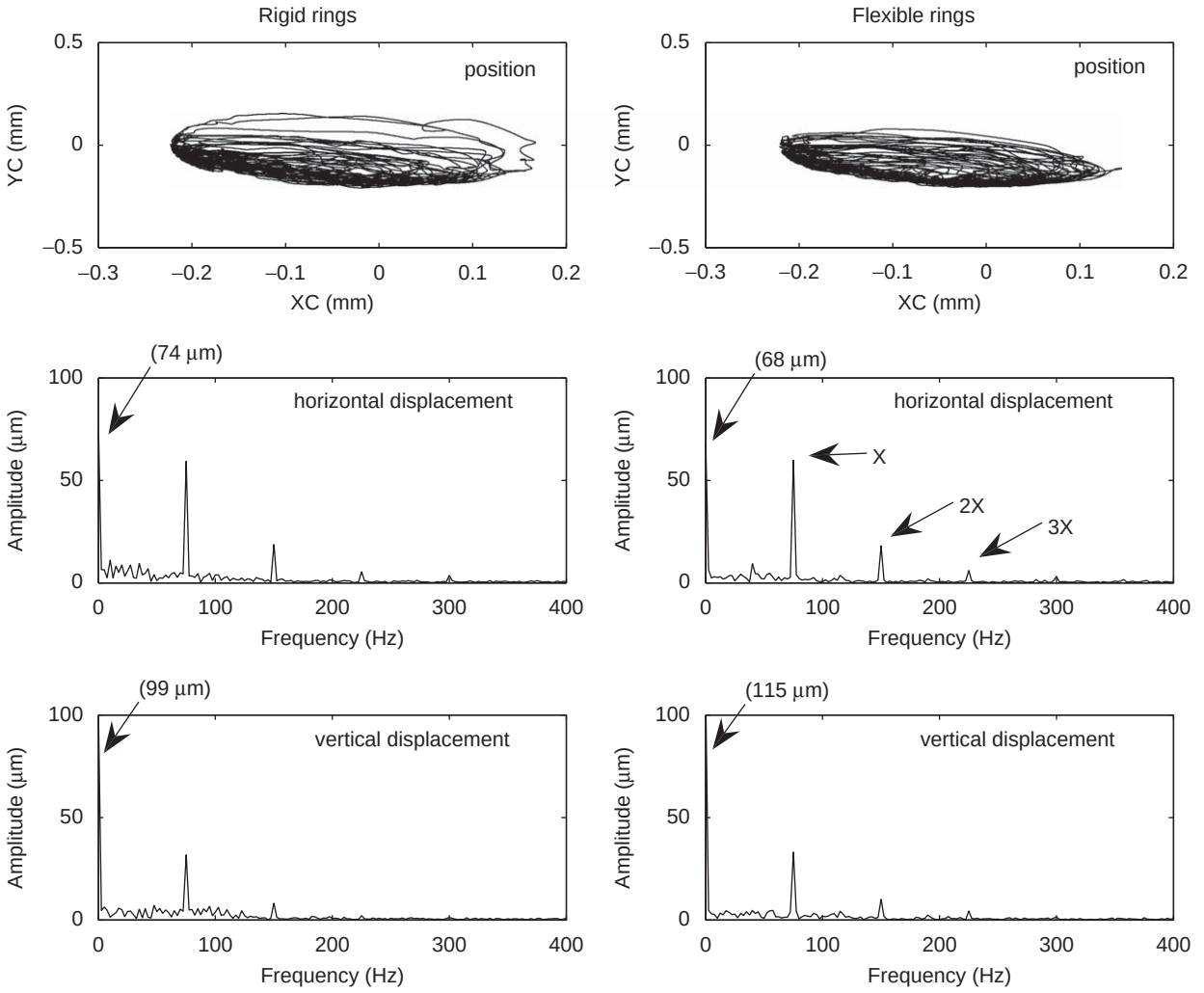

Fig. 17. Peek cage position at 4500 rev/min for $F_r = 15,000$ N—unbalanced rotor.

With a balanced rotor (cf. Figs. 14 and 15), steel and Peek cages exhibit almost the same response when the deformation of the rings is taken into account.

Their improved stability when a flexible ring is considered could be due to an increase in the clearance between the cage and the inner guiding land, which is hydrodynamically lubricated. When the rings are assumed to be rigid, the influence of the radial load is stronger, especially for the Peek cage since the first four harmonics of $(X - Y)$ appear for the vertical displacement in Fig. 15. Similarly, for an unbalanced rotor, see Figs. 16 and 17, it is observed that flexible rings have only a small effect on the cage position in comparison to rigid rings, for both steel and Peek cage materials. However, it should be underlined that the effect of the cage inertia is easy to identify: the first frequency harmonics (below X) observed in Fig. 13 are 2 or 3 times lower for a steel cage than those observed with a Peek cage (Fig. 17).

4. Conclusion

An unitary mathematical model is proposed to describe the dynamic behavior of a cylindrical roller bearing with flexible rings. Taking into account the flexibility of the rings leads to a smoother global response of the rotor-bearing assembly with less cage instabilities. Consequently, this assumption is a first-order parameter for predicting the dynamic behavior of the system. It is also found that the ball pass harmonics are significantly

modified when considering the ring flexibility. The first frequencies are more marked and the higher frequency is attenuated. Consequently, the inner ring trajectory loses one order of complexity, even with an unbalanced rotor. An inter-shaft bearing operating in a counter-rotating motion shows a larger number of frequency components: the unbalanced forces on both rings increase the nonlinearity of the system leading to many sub- and super-harmonics. These sub- and super-harmonics are found to be a linear combination of the two ring speeds. Finally, the inertia of the cage material is found to play a role on the cage trajectory.

Acknowledgments

The authors wish to acknowledge N. Weinzapfel and F. Sadeghi of the Mechanical Engineering Tribology Lab at the Purdue University for researching support.

References

[1] C.T. Walter, The dynamics of ball bearings, *Journal of Lubrication Technology—Transactions of the ASME* 93 (1971) 1–10.
[2] P.K. Gupta, Dynamics of rolling-element bearings—part I. Cylindrical roller bearing analysis, *Journal of Lubrication Technology—Transactions of the ASME* 101 (1979) 293–304.
[3] P.K. Gupta, *Advanced Dynamics of Rolling Elements*, Springer, New York, 1984.
[4] P.K. Gupta, Dynamics of rolling-element bearings—part II. Cylindrical roller bearing results, *Journal of Lubrication Technology—Transactions of the ASME* 101 (1979) 305–311.
[5] P.K. Gupta, Dynamics of rolling-element bearings—part III. Ball-bearing analysis, *Journal of Lubrication Technology—Transactions of the ASME* 101 (1979) 312–318.
[6] P.K. Gupta, Dynamics of rolling-element bearings—part IV. Ball-bearing results, *Journal of Lubrication Technology—Transactions of the ASME* 101 (1979) 319–326.
[7] C.R. Meeks, L. Tran, Ball bearing dynamic analysis using computer methods—part I: analysis, *Journal of Tribology—Transactions of the ASME* 118 (1996) 52–58.
[8] L.D. Meyer, F.F. Ahlgren, B. Weichbrodt, An analytical model for ball bearing vibrations to predict vibration response due to distributed defects, *Journal of Mechanical Design* 102 (1980) 205–210.
[9] Y.T. Su, M.H. Lin, M.S. Lee, The effects of surface irregularities on roller bearing vibrations, *Journal of Sound and Vibration* 165 (3) (1993) 455–466.
[10] R. Aini, R. Rahnejat, R. Gohar, A five degree of freedom analysis of vibrations in precision spindles, *International Journal of Machine Tools & Manufacture* 30 (1) (1990) 1–18.
[11] R.T.W.M. Hendrikx, G.C. van Nijen, P. Dietl, Vibrations in household appliances with rolling element bearings, *Proceedings of the ISMA 23 Noise and Vibration Engineering*, Vol. 3, 1998, pp. 1537–1544.
[12] Y.S. Lee, C.W. Lee, Modelling and vibration analysis of misaligned rotor–ball bearing systems, *Journal of Sound and Vibration* 224 (1999) 17–32.
[13] M. Tiwari, K. Gupta, O. Prakash, Effect of radial internal clearance of a ball bearing on the dynamics of a balanced horizontal rotor, *Journal of Sound and Vibration* 238 (2000) 723–756.
[14] M. Tiwari, K. Gupta, O. Prakash, Dynamic response of an unbalanced rotor supported on ball bearings, *Journal of Sound and Vibration* 238 (2000) 757–779.
[15] S. Harsha, K. Sandeep, R. Prakash, The effect of speed of balanced rotor on nonlinear vibrations associated with ball bearings, *International Journal of Mechanical Sciences* 45 (2003) 725–740.
[16] B. Changqing, X. Qingyu, Dynamic model of ball bearings with internal clearance and waviness, *Journal of Sound and Vibration* 294 (2006) 23–48.
[17] G. Jang, S.-W. Jeong, Vibration analysis of a rotating system due to the effect of ball bearing waviness, *Journal of Sound and Vibration* 269 (2004) 709–726.
[18] A. Palmgren, *Ball and Roller Bearing Engineering*, first ed., SKF Industries Inc., Philadelphia, 1945.
[19] G. Cavallaro, D. Nélias, F. Bon, Analysis of high-speed inter-shaft cylindrical roller bearing with flexible rings, *Tribology Transactions* 48 (2) (2005) 154–164.
[20] A. Hirotoshi, S. Yoshio, M. Yuka, S. Takeshi, Performance of ball bearings with silicon nitride ceramic balls in high speed spindles for machine tools, *Journal of Tribology—Transactions of the ASME* 110 (4) (1988) 693–698.
[21] W.C. Young, R.G. Budynas, *Roark's Formulas for Stress and Strain*, seventh ed., McGraw-Hill, New York, 2002.
[22] J.A. Wensing, On the Dynamics of Ball Bearings, Ph.D. Thesis, University of Twente, Enschede, The Netherlands, December 1998.
[23] N. Ghaisas, C.R. Wassgren, F. Sadeghi, Cage instabilities in cylindrical roller bearings, *Journal of Tribology—Transactions of the ASME* 126 (2004) 681–689.